JES Focus Issue on Redox Flow Batteries—Reversible Fuel Cells

High Active Surface Area and Durable Multi-Wall Carbon Nanotube-Based Electrodes for the Bromine Reactions in H_2-Br_2 Fuel Cells

Venkata Yarlagadda,[a,*] Guangyu Lin,[b,] Pau Ying Chong,[b] and Trung Van Nguyen[a,***,z]**

[a]*Department of Chemical and Petroleum Engineering, The University of Kansas, Lawrence, Kansas 66045, USA*
[b]*TVN Systems, Inc., Lawrence, Kansas 66046, USA*

The commercially available carbon gas diffusion electrodes (GDEs) with low specific active area but high permeability are often used as Br_2 electrodes in the H_2-Br_2 fuel cell. In order to increase the specific active surface area of the existing carbon GDEs, a study was conducted to grow multi-wall carbon nanotubes (MWCNTs) directly on the surface of carbon fibers of a commercial carbon electrode. Experimental fixtures were developed to promote the electrodeposition of cobalt and the growth of MWCNTs on the carbon GDE. The MWCNT growth across the carbon electrode was confirmed by SEM. The carbon GDE with a dense distribution of short MWCNTs evaluated in a H_2-Br_2 fuel cell has 29 times higher active surface area than a plain carbon electrode and was found to be highly durable at an electrolyte flow rate of 10 cc/min/cm^2. The performance of the best single layer MWCNT GDE measured at 80% discharge voltage efficiency in a H_2-Br_2 fuel cell was found to be 16% higher compared to that obtained using three layers of plain carbon electrodes. Finally, the preliminary material cost analysis has shown that the MWCNT-based carbon electrodes offer significant cost advantages over the plain carbon electrodes.

Manuscript submitted August 17, 2015; revised manuscript received October 16, 2015. Published October 30, 2015. This was Paper 682 presented at the Chicago, Illinois, Meeting of the Society, May 24–28, 2015. *This paper is part of the JES Focus Issue on Redox Flow Batteries–Reversible Fuel Cells.*

The regenerative hydrogen-bromine (H_2-Br_2) fuel cell is one of the potential candidates for large scale electrical energy storage.[1–8,11] However, there are three major material related challenges that need to be addressed in order to make the H_2-Br_2 fuel cell system more viable. First, a membrane that restricts the crossover of unwanted bromine species (Br_2, Br^-, and Br_3^-) from the bromine electrode to the hydrogen electrode is required. Second, an active H_2 electrocatalyst that is stable in hydrobromic acid (HBr)/bromine (Br_2) is needed. Third, bromine electrodes with high active surface area are desired. Prior works conducted in this area have explored novel H_2 electrocatalyst and membrane materials that could possibly replace the conventionally used platinum (Pt)/carbon (C) catalyst and Nafion membrane used in the H_2-Br_2 fuel cell system.[9–13] Also, a previous study conducted by our group has introduced multi-wall carbon nanotube (MWCNT)-based carbon electrodes with high specific active surface area as an alternative to the widely used plain carbon Br_2 electrodes.[14,15]

Several research investigations reported in the literature have successfully grown MWCNTs directly on the carbon electrode fiber surface.[16–19] These MWCNT-based electrodes were successfully employed in polymer electrolyte membrane (PEM) fuel cells. The MWCNTs were grown on the surface of the GDE, and subsequently platinum (Pt) was electrodeposited in order to improve the catalyst utilization in the PEM fuel cell.[16] The electronic pathways were secured by depositing Pt nanoparticles directly on the MWCNTs, thus improving the catalyst utilization. On the other hand, the bromine reactions in H_2-Br_2 fuel cells don't require expensive metal catalysts and hence plain carbon GDEs with high specific active surface area are often used.[6] In order to increase the specific active surface area of existing GDEs, it is crucial to grow MWCNTs not only on the outer surface but also in the cross-section of the GDE. The cross-sectional area in these plain carbon GDEs can be accessed by employing an interdigitated flow-field design in the H_2-Br_2 fuel cell.[20] For example, Barton et al. synthesized MWCNT Toray carbon electrodes to improve the electrochemical performance of biocatalytic electrodes by using an experimental configuration that promotes nanotube growth in the cross-section of the carbon GDE.[19]

Since the majority of the active surface area is present inside (cross section) the porous carbon GDE, it is important to have MWCNT growth over the entire carbon electrode fiber surface area. The major limitation associated with the synthesis of MWCNT-based carbon electrodes by electrodeposition described in our previous study is that the MWCNT growth is non-uniform and occurs mostly on the fibers near the outer surfaces of the carbon electrode.[15] The non-uniform MWCNT growth arises from the non-uniform electrodeposition of Co nanoparticles as a result of the poor current collection. Hence, a new experimental approach where the current collection was done normal to the surface of the carbon electrodes to improve the electrodeposition of Co nanoparticles inside the carbon electrode is needed. Also, a new experimental fixture that promotes MWCNT growth inside the carbon electrode is equally important.

The following studies are discussed in this paper:

1. The synthesis of MWCNT-based carbon electrodes using modified electrodeposition and chemical vapor deposition experimental set-ups,
2. The durability of MWCNT GDEs against high liquid flow rates by measuring their active surface area before and after operating in the electrolyte flow through mode with an interdigitated flow field,
3. The optimization process implemented to synthesize electrodes with durable high-density and short-length MWCNTs,
4. The performance of MWCNT-based electrodes as compared to conventional carbon electrodes in a H_2-Br_2 fuel cell,
5. The fluid pressure drop across both the plain and the MWCNT-based carbon electrodes, and
6. A material cost analysis highlighting the cost benefits of using MWCNT-based carbon electrodes versus of multiple plain carbon electrodes in a H_2-Br_2 fuel cell.

Experimental

Synthesis of MWCNT-based carbon electrodes using flow-through based experimental fixtures.— A two-electrode arrangement was used to implement the pulse current electrodeposition technique. The

*Electrochemical Society Student Member.
**Electrochemical Society Active Member.
***Electrochemical Society Fellow.
[z]E-mail: cptvn@ku.edu

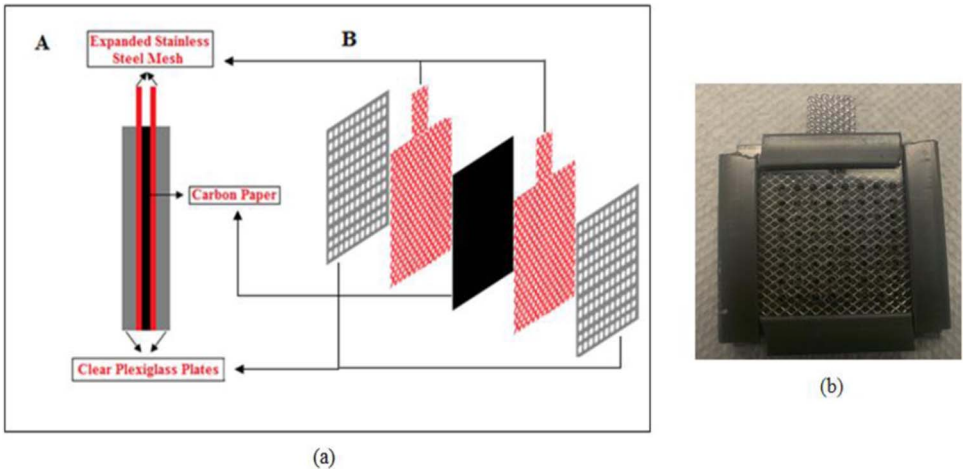

Figure 1. a) Working electrode fixture (A. Side view and B. 3D view) used in the electrodeposition experiment and b) Finished working electrode fixture.

carbon electrodes were boiled in DI water and soaked in a solution of cobalt sulfate and boric acid prior to electrodepositing the Co nanoparticles. The whole electrodeposition process remains the same as described in our prior work except for the working electrode configuration.[15] The stainless steel alligator clips were replaced by expanded stainless steel mesh current collectors.

As shown in Figure 1a, the carbon electrode was sandwiched between two expanded stainless steel mesh (67%–75% open area) current collectors and the resulting fixture was enclosed between perforated Plexiglas (5 mm thick with multiple 2 mm diameter openings) plates. Finally, chemically resistant Nylon sleeves (McMaster Carr) were slid across the sides of the fixture to provide uniform compression in the normal direction. The assembled experimental fixture was then placed in the electrolyte solution and pulse current electrodeposition was carried out to deposit Co nanoparticles. The stainless steel mesh provided uniform current collection as it covered the entire carbon electrode surface. The openings in the Plexiglas plates and stainless steel mesh allowed the carbon electrode to access the electrolyte solution. The new electrodeposition fixture assisted in providing better cobalt ions access and good electronic conductivity and connectivity to all carbon fibers in the electrode. The dimensions of the carbon electrodes, expanded stainless steel mesh, and perforated Plexiglas plates were 5 cm by 5 cm. Figure 1b shows the working electrode fixture used in this study.

The Co nanoparticles were electrodeposited by applying a cathodic pulse current to the working electrode. The pulse current technique offered an additional advantage over the constant current technique since it provided better control over the particle size and distribution of the metal catalyst electrodeposited onto the carbon substrate.[21] The effect of precursor solution concentration on the size and distribution of Co nanoparticles was examined by using two different solution mixtures (A and B). Solution A was a mixture of 0.02 M $CoSO_4$ and 0.33 M H_3BO_3. Solution B was a mixture of 0.01 M $CoSO_4$ and 0.16 M H_3BO_3. A cathodic pulse current of −30 mA was applied for 1 second when solution A was used. A total of 5 and 15 pulses were used to synthesize sample 1 and sample 2 respectively using solution A. A cathodic pulse current of −10 mA was applied for 1 second when solution B was used. A total of 45 pulses were used to synthesize sample 3 using solution B. The solutions were stirred during the rest time (1 minute) in between the pulses to replenish the electrolyte concentration near the electrode/electrolyte interface. The geometric area of all the samples was 25 cm^2. After electrodepositing Co, the carbon electrodes were soaked in liquid nitrogen for 15 minutes to make them hard and brittle. A small piece of carbon electrode was then broken and the exposed cross section was subsequently analyzed using Scanning Electron Microscopy (SEM).

The experimental procedure for growing MWCNTs on the carbon electrode fiber surface was similar to the one described in our prior work.[15] The only variation was that the carbon electrodes were enclosed in a fixture to promote MWCNT growth inside the carbon electrode. In order to force the gas mixture through the carbon electrode, the experimental fixture shown in Figure 2 was placed inside the quartz tube. As shown in Figure 2a (side view), the experimental setup consisted of two dense alumina foam blocks with carbon paper inserted in between them. The diameter of alumina foam blocks approximately matched the inner diameter of the quartz tube. Alumina foam blocks used in the experimental fixture are shown in Figure 2b. The side of alumina foam blocks facing the carbon paper (shown in view 1) consisted of a thin vertical slit and multiple openings. The carbon paper was inserted into the vertical slit and the openings served as gas-flow channels. The depth of the vertical slit was equal to half the thickness of the alumina foam block whereas the gas-flow channels run all the way through the foam blocks. View 2 in Figure 2b shows the side of the foam blocks facing the quartz tube inlet and outlet, respectively. The gas-flow channels were machined to the right side of one of the alumina foam blocks and to the left side on the other to force the gas to flow through the porous carbon electrode. The top view shown in Figure 2c depicts the gas flowing through the carbon electrode. This promotes the MWCNT growth inside the carbon electrode. The experimental fixture was placed in a quartz tube and subsequently inserted into the quartz tube furnace to grow MWCNTs.

The CVD process used to grow MWCNTs was similar to the one described in our previous work except for the reaction temperature and flow rates of C_2H_2, Ar, and H_2.[15] The temperature used for growing MWCNTs was increased from 700°C to 750°C. The MWCNT growth rate increases as the temperature increases. The flow rate was increased since the quartz tube with a larger diameter (44 mm inner diameter) was used instead of the one with a smaller diameter (20 mm inner diameter) used for the studies discussed in our prior work.[15] We used a large quartz tube in this study to make larger samples. The flow rates for C_2H_2, Ar, and 20% H_2/Ar mixture were 20 cc/min, 170 cc/min, and 180 cc/min, respectively. The resulting gas mixture was composed of 9.7% H_2, 5.4% C_2H_2, and 84.9% Ar. The MWCNT-based carbon electrodes were soaked in liquid nitrogen and broken to analyzing their cross-sectional area using SEM. The post-treatment and electrochemical analysis (enhancement factor measurements) procedures were described in detail in our previous work.[15] The only change made in this study was that the MWCNT-based carbon electrodes were boiled in DI water in order to make them hydrophilic before testing them in a H_2-Br_2 fuel cell.

Durability, fuel cell performance and pressure drop measurements.— The effect of fluid shear on the active surface area of MWCNT electrodes was conducted in a 1 cm^2 H_2-Br_2 fuel cell at room temperature (~22°C) to determine the durability of the MWCNT-based electrodes against high liquid flow rates under

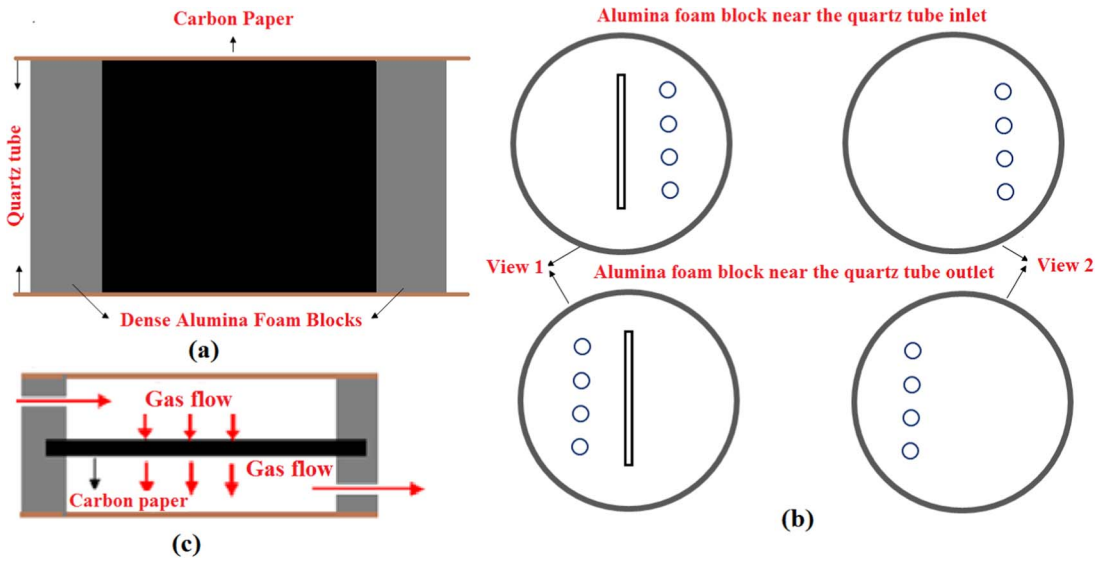

Figure 2. Experimental set-up used to perform CVD (a. Side view, b. Front view, and c. Top View).

the flow-through mode. The fuel cell and membrane electrode assembly configurations were described in detail in our previous communication.[11] A 1 M HBr/0.1 M Br_2 electrolyte was fed to the bromine electrode and humidified H_2 gas was recirculated through the hydrogen electrode. The flow rates of HBr/Br_2 solution and H_2 gas were 10 cc/min/cm^2 and 1030 cc/min respectively. Polarization curves were obtained using multi-step chronoamperometry with applied overpotentials ranging between +24 mV and −24 mV and the dI/dV slopes were collected until the slope appeared to level off. Based on the linearized Butler-Volmer equation, the dI/dV slope is directly correlated to the product of active surface area (a) and exchange current density (i_o).[7] The dI/dV slope of the MWCNT-based electrode was normalized to that of a plain SGL 10AA carbon electrode to calculate the active surface area enhancement factor. The initial polarization curve and dI/dV slope were measured after flowing the HBr/Br_2 electrolyte for 15 min. Both HBr/Br_2 solution and the humidified H_2 gas were recirculated continuously throughout the entire experiment. The difference between the initial and final enhancement factors or dI/dV slopes determines the percentage loss of multi-wall carbon nanotubes (MWCNTs) due to continuous fluid shear.

A plain 0.1245 cm thick electrode (3 pieces of SGL 10AA stacked together) and a 0.0415 cm thick MWCNT-based carbon electrode (1 piece of SGL 10AA) as Br_2 electrodes were evaluated in a H_2-Br_2 fuel cell. A SGL 25BC electrode with Pt catalyst coating (catalyst loading between 0.4 and 0.45 mg-Pt/cm^2) obtained from TVN systems, Inc. was used as the H_2 electrode. The MEAs were made by hot pressing Pt coated SGL 25 BC electrodes onto Nafion 212 membranes at a temperature of 135°C for 5 minutes. These MEAs were later boiled in DI water for 30 minutes to hydrate the Nafion ionomer present in the membrane electrode assembly (MEA). The operating conditions for the fuel cell performance measurements are specified as follows. A mixture of 2 M HBr and 0.9 M Br_2 was recirculated through the Br_2 electrode at multiple flow rates (1, 2, 5, 7, and 10 cc/min/cm^2). Humidified H_2 gas at a flow rate of 40 cc/min was pumped through the H_2 electrode and vented out at ambient pressure. All the fuel cell experiments were conducted at room temperature (∼22°C) unless otherwise specified. The internal ohmic resistance of the fuel cell was measured using Electrochemical Impedance Spectroscopy (Gamry EIS 300, Amplitude: 5 mV and Frequency range: 0.1 Hz to 100 kHz).

The pressure drop caused by fluid flow through the plain and the MWCNT-based electrodes was measured using a U-tube water manometer placed between the inlet and the outlet of the flow field plate located next to the Br_2 electrode. A plastic sheet was used instead of the membrane to seal (or secure) the H_2 electrode compartment in the fuel cell. Both plain and MWCNT-based carbon electrodes were used as the Br_2 electrodes. Water was pumped through the Br_2 side and the height differential of the liquid columns between the two legs of the manometer was measured. The pressure drop (in cm H_2O) was measured at different water flow rates.

Cost analysis.— The cost analysis was performed to compare the cost of MWCNT electrodes to that of plain carbon electrodes (3 pieces of SGL 10AA). The cost analysis is preliminary since it only includes the processing, synthesis materials and electrode costs. The combined cost of electrodeposition and CVD processes would contribute toward the total cost of MWCNT electrode synthesis. The cost of cobalt sulfate ($CoSO_4$), boric acid (H_3BO_3), and electricity constitutes the total cost of electrodeposition process. The cost of acetylene, argon, hydrogen, and electricity constitute the total cost of CVD process. A case study was conducted to illustrate the cost benefits associated with using MWCNT-based carbon electrodes in a H_2-Br_2 fuel cell.

Results and Discussion

Electrodeposition of Co nanoparticles.— Initially, the electrodeposition of Co nanoparticles was done using solution A (0.02 M $CoSO_4$ and 0.33 M H_3BO_3). The electrodeposition current, time and number of pulses were listed in the Experimental section. The SEM images of cross sectional area of the porous carbon electrodes after electrodepositing Co are shown in Figures 3a and 3b. The images on the right in Figures 3a and 3b are magnified 9 times compared to the ones on the left to highlight the presence of Co nanoparticles on the carbon fiber substrate. As the electrodeposition time increases from 5 to 15 seconds, while applying the same pulse current magnitude, the density of Co nanoparticles increases. The fact that Co nanoparticles were successfully electrodeposited inside the carbon electrode (cross section) shows the benefit of using stainless steel mesh current collectors. The diameter of the Co nanoparticles was between 30 and 70 nm.

MWCNT growth using CVD process.— After electrodepositing Co, carbon electrodes were inserted into the fixture shown in Figure 2 and then placed inside the quartz oven to grow MWCNTs. The MWCNTs were grown at 750°C for 45 min in the flow of C_2H_2, Ar and H_2. The SEM images of the electrode cross section of samples 1 and 2 after growing MWCNTs are shown in Figure 4. As shown in Figures 4a and 4b, the MWCNT growth was successfully accomplished in the electrode cross section, which was a result of the flow-through

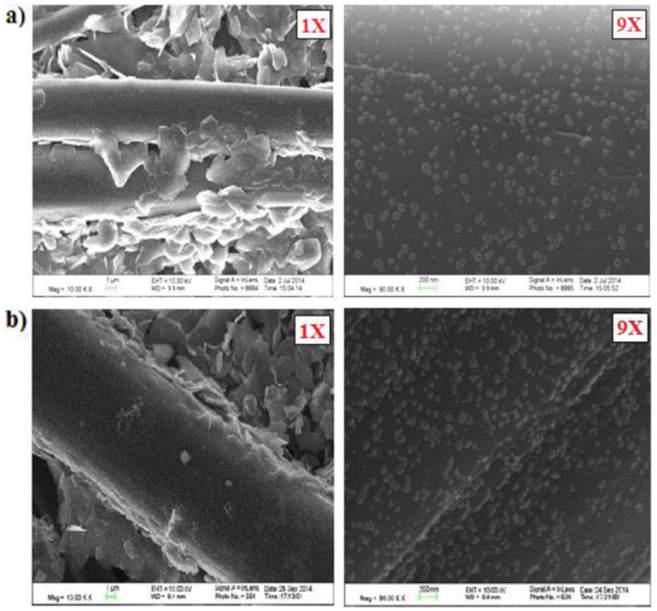

Figure 3. SEM analysis of carbon electrode cross-section after electrodepositing of Co a) −30 mA for 5s (sample 1) and b) −30 mA for 15s (sample 2).

condition created by the experimental fixture used in this study. The dense Co nanoparticle distribution seen in sample 2 (−30 mA for 15s) contributed toward the dense nanotube growth as shown in Figure 4b. The MWCNT-based carbon electrodes were then boiled in DI water and soaked in 2 M HBr solution overnight to remove amorphous carbon impurities and exposed Co nanoparticles before measuring their active surface area enhancement factors.

Surface area enhancement and durability measurements.— The active surface area enhancement factors of MWCNT electrodes were measured in a solution of 1 M HBr and 0.1 M Br_2 using a three-electrode arrangement as described in our earlier work.[14,15] Figure 5

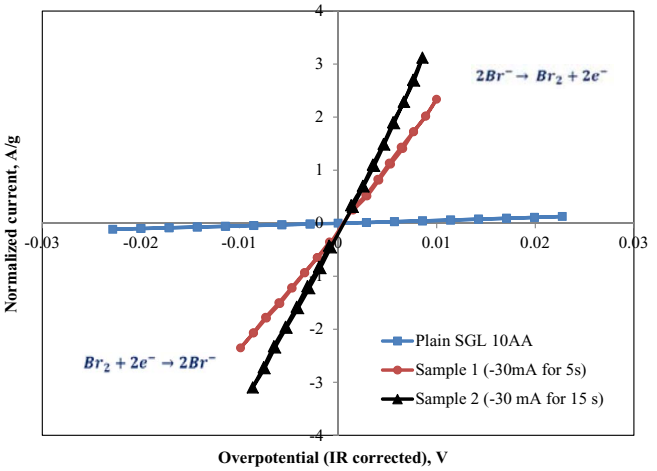

Figure 5. Multi-step chronoamperometry curves of MWCNT-based electrodes in a three-electrode arrangement (samples 1 and 2).

Table I. Active surface area enhancement factors (CVD synthesis time of 45 minutes).

Specimen	Enhancement factor
Sample 1	44
Sample 2	67

shows the multi-step chronoamperometry curves obtained with a plain SGL 10AA carbon electrode, sample 1, and sample 2. The product of active surface area (a) and exchange current density (i_o) was obtained using the linearized Butler-Volmer equation.[7] As shown in Table I, the active surface area enhancement factors for samples 1 and 2 are 44 and 67, respectively. As expected, the active surface area of sample 2 was higher compared to that of sample 1 because of its dense MWCNT growth.

During the CVD process, the length and density of MWCNTs can be controlled by varying the parameters such as synthesis time, acetylene concentration, and synthesis temperature. In this study, the effect

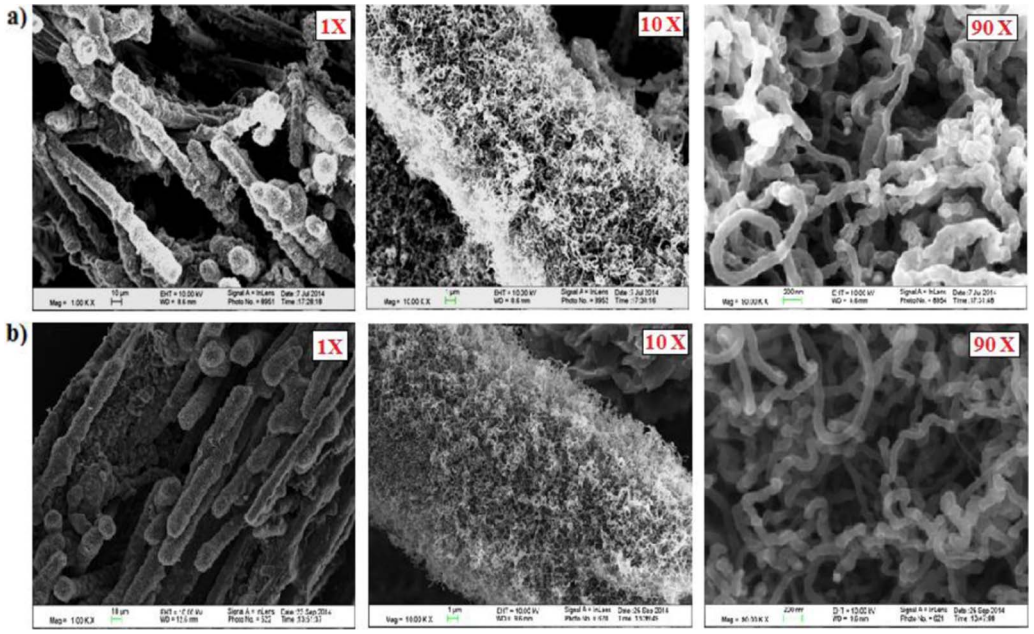

Figure 4. SEM images of cross-section of MWCNT-based electrodes (synthesized at 750°C for 45 min), under different magnifications (a: sample 1 and b: sample 2).

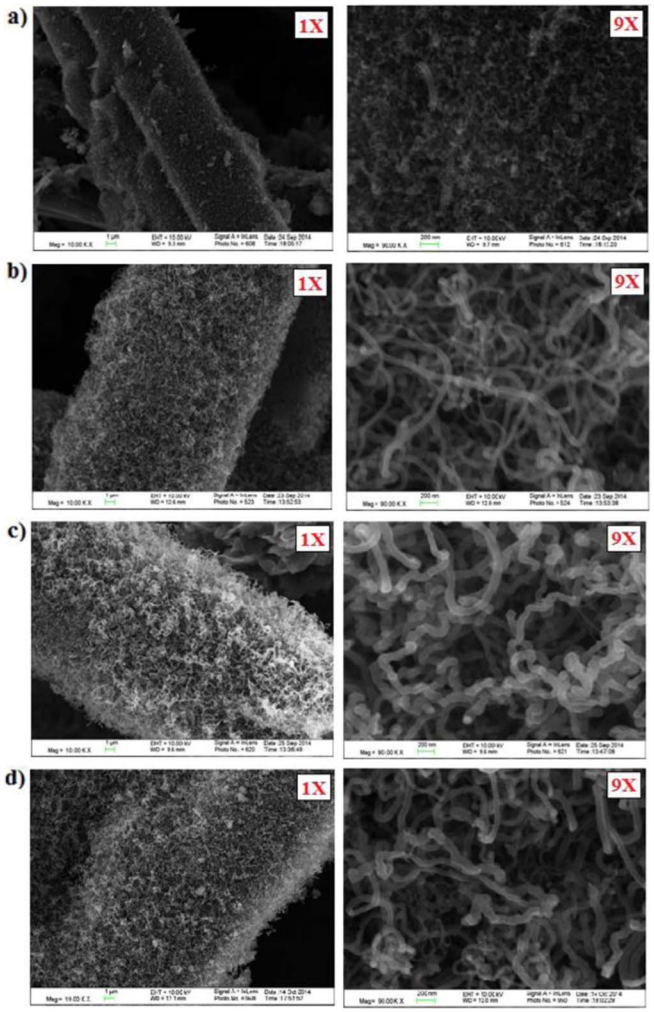

Figure 6. SEM images of a cross-section of MWCNT-based electrodes produced using sample 2 and different CVD synthesis times (min.): a. CVD 15, b. CVD 30, c. CVD 45, and d. CVD 60.

of synthesis time on the active surface area of porous carbon electrodes was examined, while maintaining a constant acetylene concentration and reaction temperature (750°C). Sample 2 was chosen for this study because of its high active surface area. The MWCNTs were grown on sample 2 at different CVD synthesis times (15, 30, 45, and 60 minutes). Based on the CVD synthesis time, the samples were labeled as CVD 15, CVD 30, CVD 45, and CVD 60 respectively. Figure 6 shows the SEM images of the samples after growing MWCNTs at different synthesis times. The length and density of MWCNTs increased as the CVD synthesis time increased from 15 to 60 minutes. Beyond a certain length, the MWCNTs bent on their own weight and became tangled as shown in Figure 6. One of the advantages of tangled MWCNTs was their increased durability when exposed to high liquid flow rates. However, the tall nanotubes might block the pores in the carbon electrodes, which in turn might result in a larger pressure drop. Long nanotubes also restrict the electrolyte to access to the internal surface area (or cross sectional area) of the porous carbon electrode. Since, a flow-through tantalum flow field plate was used in the Br_2 electrode, the active surface area present inside (cross sectional area) the MWCNT-based carbon electrode played an important role in determining its performance. Hence, it was critical to test these MWCNT-based electrodes in a fuel cell at high flow rates to determine their durability and performance.

The multi-step chronoamperometry curves and active surface area enhancement factors of MWCNT-based carbon electrodes obtained

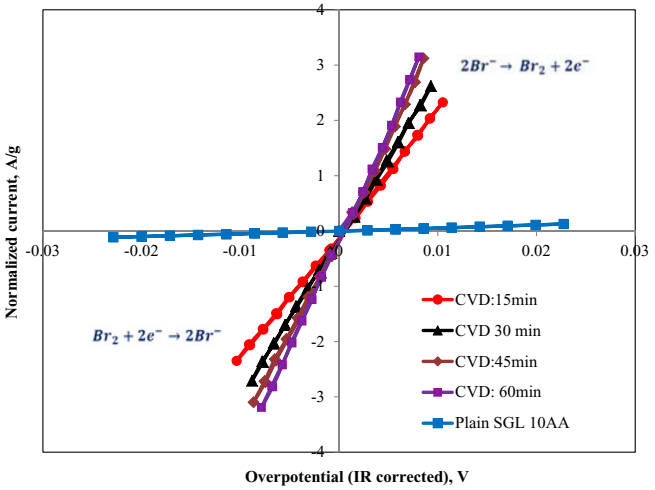

Figure 7. Multi-step chronoamperometry curves of MWCNT-based electrodes generated at different CVD synthesis times in a three-electrode arrangement (CVD 15, CVD 30, CVD 45, and CVD 60).

at different CVD synthesis times are shown in Figure 7 and Table II respectively. The active area of the MWCNT-based carbon electrodes increased as the CVD synthesis time increased (active surface area enhancement factors between 43 and 75 were achieved). The main difference with measuring enhancement factors in a fuel cell versus in a three-electrode arrangement is that the bromine reaction can also occur on the electrically conductive flow field surface resulting in a higher current. However, as long as one compares the data obtained from the same setup (i.e., fuel cell data to fuel cell data or three-electrode data to three-electrode data) this difference does not matter.

As described in the Experimental section, the durability measurements were conducted in a H_2-Br_2 fuel cell. The flow rates of HBr/Br_2 electrolyte and H_2 were specified in the experimental section. The dI/dV slope was measured periodically while maintaining continuous HBr/Br_2 and H_2 recirculation. Initially, a plain SGL 10AA carbon electrode was tested in a H_2-Br_2 fuel cell to ensure that there was no effect of HBr/Br_2 crossover on the fuel cell performance over an extended period (7 hours). As shown in Figure 8, reproducible polarization curves were obtained over 7 hours of testing, which shows that there was no noticeable HBr/Br_2 or H_2 crossover within the duration of testing. Also, the specific currents obtained using a H_2-Br_2 fuel cell with the plain SGL 10AA carbon electrode are higher compared to that obtained using a three-electrode arrangement. This difference can be attributed to the bromine reaction occurring on the surface of the conductive flow field plate as explained earlier. The durability results from the fluid shear experiment for the MWCNT-based carbon electrodes are shown in Figures 9a and 9b and Table III.

Figure 9a shows the dI/dV slopes measured as a function of time whereas Figure 9b shows the initial (after 15 min) and final (7–9 hours later) polarization curves. The initial and final enhancement factors are shown in Table III. Two observations were noted in the durability test. First, the surface areas of MWCNT-based carbon electrodes decreased as soon as the electrodes were subjected to high fluid shear stress. This initial decrease in active surface areas was as much as

Table II. Active surface area enhancement factors of MWCNT-based electrodes at different CVD synthesis times.

Specimen	Enhancement factor
CVD 15	43
CVD 30	55
CVD 45	67
CVD 60	75

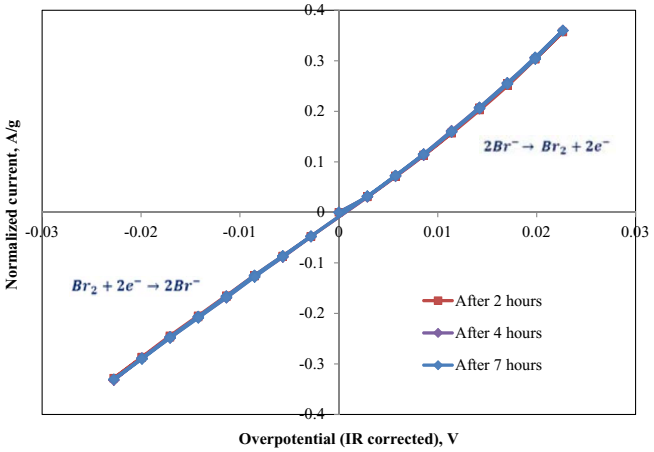

Figure 8. Effect of exposure to constant shear rate on a plain SGL 10AA carbon electrode.

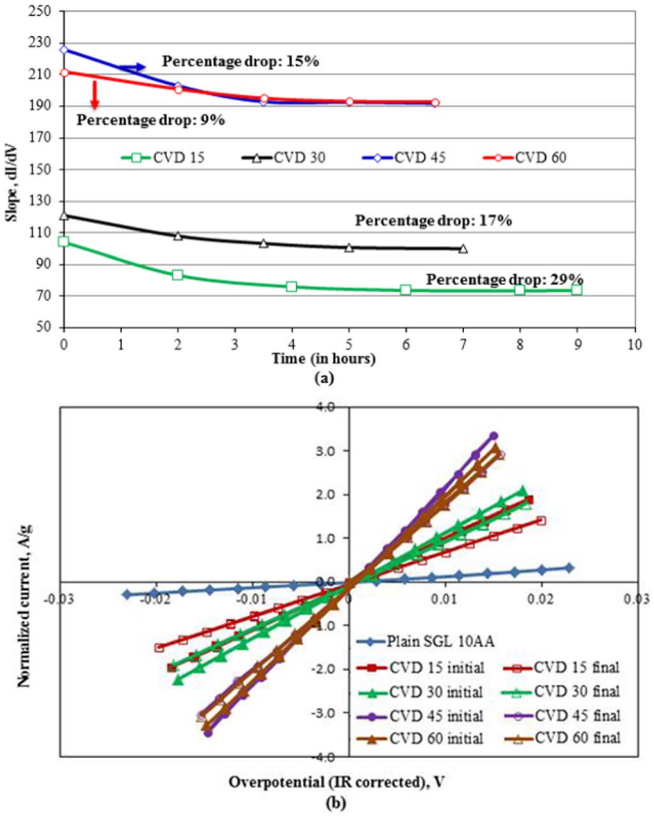

Figure 9. Effect of exposure to constant shear rate on the surface area of CNT electrodes treated at different CVD times (a) changes in the dI/dV slope (surface activity) as the samples were subjected to continuous shear rate (b) initial and final (7–9 hrs. later) polarization curves.

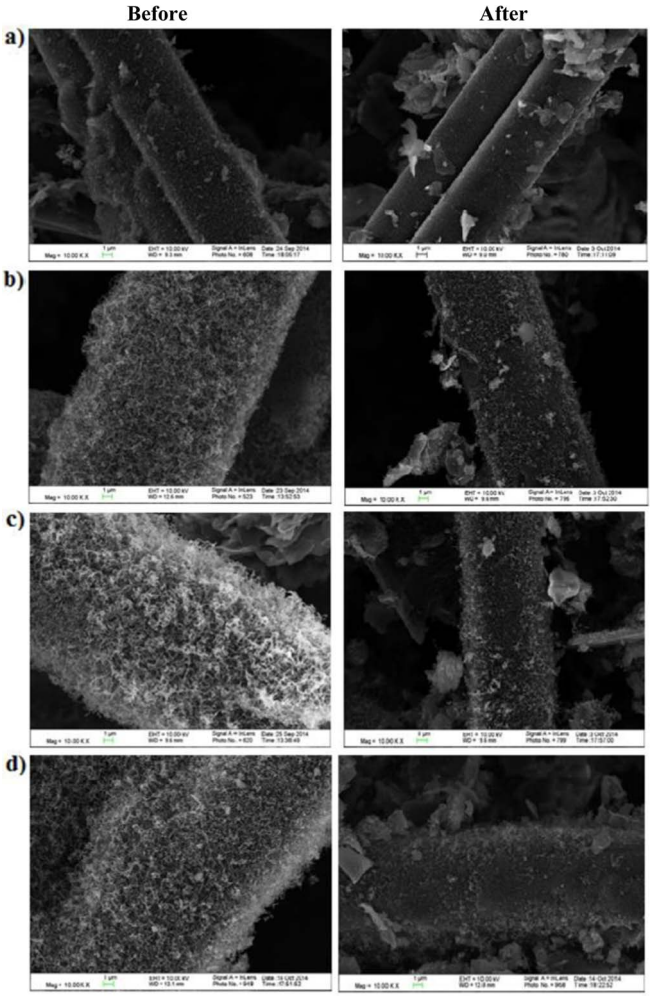

Figure 10. SEM images of the cross-section of a MWCNT electrodes before and after the durability test (a. CVD 15, b. CVD 30, c. CVD 45, and d. CVD 60).

70% (shown in Table III), which is determined by comparing the enhancement factor obtained from the three electrode arrangement and the initial slope (dI/dV) measured after 15 min from the durability study. Second, after this initial loss in surface area, additional loss during prolonged operation was minimal, especially with electrodes with longer MWCNTs. The carbon electrodes with long and dense MWCNTs were able to withstand high liquid flow rates as shown in Table III (percentage drop in surface area decreased from 29% to 9% as the CVD synthesis time increased from 15 to 60 min). The results also show that longer CNTs created beyond 45 minutes of CVD did not contribute to an additional increase in active surface area. The final surface areas after the durability test are still much higher than that of conventional carbon electrodes. The SEM images of MWCNT-based carbon electrodes before and after the shear test are shown in Figure 10.

The location where the MWCNT bends on its own weight is very fragile. The part of the MWCNT beyond the bend is vulnerable and can

Table III. Summary of effect of fluid shear rate on surface enhancement factor of MWCNT electrodes.

Specimen	Enhancement factor (three-electrode set up)	Initial enhancement factor	Final enhancement factor	Percentage drop
CVD 15	43	8X	5.6X	29%
CVD 30	55	9.3X	7.7X	17%
CVD 45	67	17.3X	14.7X	15%
CVD 60	75	16.2X	14.8X	9%

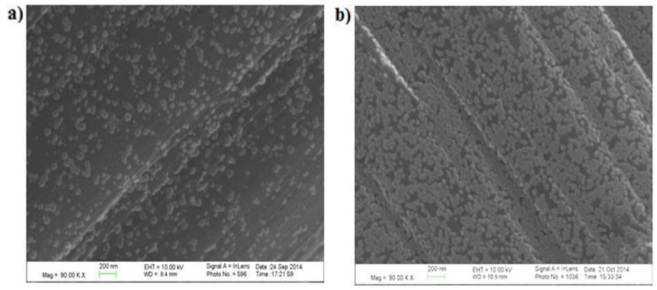

Figure 11. Effect of $CoSO_4$ concentration on the diameter and density of Co nanoparticles (a. sample 2: 0.33 M $CoSO_4$ and b. sample 3: 0.16 M $CoSO_4$).

be severed at high liquid flow rates. As shown in Figure 10, a certain percentage of MWCNTs is lost, leaving behind short MWCNTs on the carbon electrode fiber surface for all the four samples synthesized at different durations using the CVD process (samples: CVD 15, CVD 30, CVD 45, and CVD 60). Note that, after the long MWCNTs were truncated, one could see that a large fraction of the carbon fiber surface area was still available for additional CNT growth. In the following sections, the optimized electrodeposition process that produces dense MWCNTs is discussed.

Synthesis of short, dense MWCNTs.— As seen in Figure 10, long MWCNTs were truncated once they were subjected to high liquid flow rates. Hence, a reasonable way to improve the durability of MWCNT-based carbon electrodes was to grow short, dense MWCNTs on the electrode fiber surface. As the density of MWCNT distribution increases, the active surface area of the MWCNT-based carbon electrode improves as well. One way to improve the MWCNT density is by modifying the electrodeposition conditions to generate small Co nanoparticles with dense distribution. The optimized electrodeposition conditions along with SEM and electrochemical analysis are discussed in the following sections.

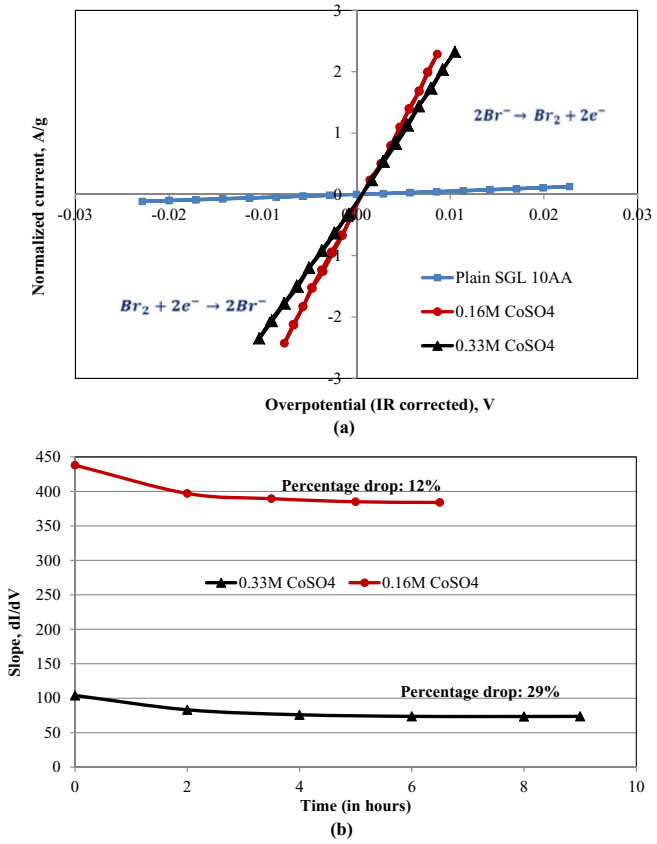

Figure 12. a) Effect of $CoSO_4$ concentration on active area enhancement factors and b) Effect of exposure to constant shear rate on the surface area of MWCNT electrodes synthesized at different $CoSO_4$ concentrations (sample 2: 0.33 M $CoSO_4$ and sample 3: 0.16 M $CoSO_4$).

Table IV. Active surface area enhancement factors of samples synthesized at different $CoSO_4$ concentrations.

Specimen	Enhancement factor
Sample 2 (0.33 M $CoSO_4$)	43
Sample 3 (0.16 M $CoSO_4$)	54

The $CoSO_4$ and H_3BO_3 concentration in solution A specified in the Experimental section was reduced to half (solution B) and subsequently Co was electrodeposited. Sample 3 (−10 mA applied for 45 seconds) was synthesized using solution B (0.01 M $CoSO_4$ and 0.16 M H_3BO_3). Figure 11 shows the SEM images of samples 2 and 3 after electrodepositing Co. The concentration of $CoSO_4$ determines the number of moles of Co available in the solution near the electrode surface. As expected, the diameter of Co nanoparticles decreased as the concentration of Co decreased in the solution used for electrodeposition (seen in Figure 11). Also, the density of Co nanoparticles was high in sample 3, which in turn aids in obtaining dense MWCNT distribution. The MWCNTs were grown on sample 3 using the same conditions described previously. Since previous durability measurements indicated that tall MWCNTs will be lost at high liquid flow rates, the CVD synthesis time for sample 3 in this study was reduced to 15 minutes in order to grow short MWCNTs. Subsequently, the active surface area enhancement factor and durability of sample 3 were measured.

Figures 12a and 12b compare the enhancement factors and durability measurements of samples 2 and 3 (MWCNTs were synthesized at 750°C for 15 minutes). The active surface area enhancement factor of sample 3 is 20% higher than that of sample 2 (labeled as CVD 15) as shown in Figure 12a and Table IV. Two observations were noted from the shear measurements shown in Figure 12b. First, the resistance of MWCNTs against high liquid electrolyte flow rate is higher for sample 3 as shown in Figure 12b (12% drop in surface area of sample 3 compared to 29% drop in surface area of sample 2). This might be a result of dense MWCNT growth obtained in sample 3 (shown in Figure 13), which is directly correlated to its dense Co nanoparticle distribution. Second, the active surface area of sample 3 after subjecting it to fluid shear stress is still 5 times higher than that of sample 2 (shown in Table V). As shown in Figure 13, a large amount of the short MWCNTs still remain on sample 3. Finally, sample 2 (CVD 45: synthesized at 750°C for 45 minutes) and sample 3 (synthesized at 750°C for 15 minutes) were tested in a H_2-Br_2 fuel cell to determine their performance.

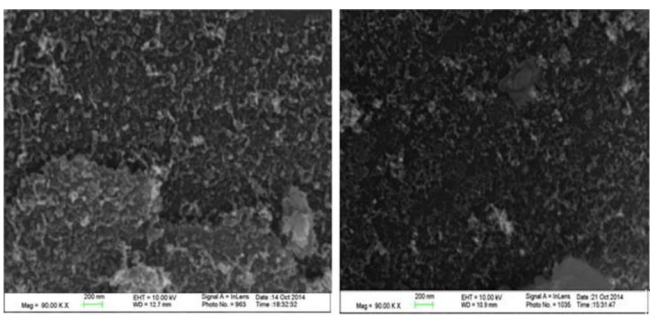

Figure 13. Sample 3 (synthesized using 0.16 M $CoSO_4$) before (left) and after (right) shear measurements.

Table V. Durability measurements of samples synthesized using different $CoSO_4$ concentrations.

Specimen	Enhancement factor (three-electrode set up)	Initial enhancement factor	Final enhancement factor	Percentage drop
Sample 2 (0.33 M $CoSO_4$)	43	8X	5.6X	29%
Sample 3 (0.16 M $CoSO_4$)	54	33X	29X	12%

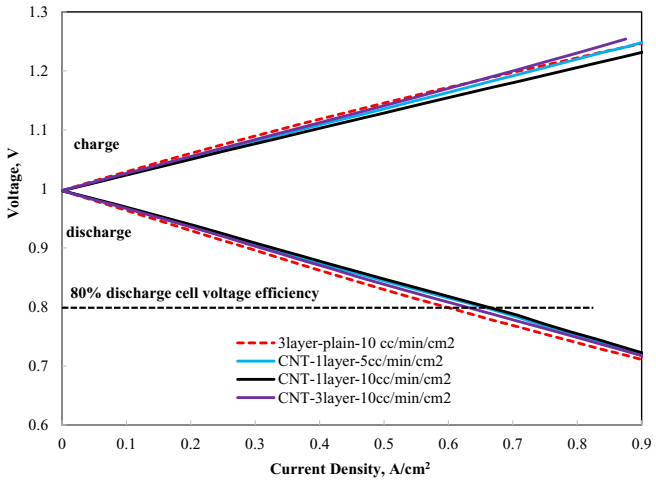

Figure 14. Polarization curves measured during charge and discharge with 3 layers of conventional electrode and 1 layer and 3 layers of MWCNT electrode (Sample 2: CVD 45) at different HBr/Br_2 flow rates.

Fuel cell measurements.— The synthesized MWCNT electrodes were tested in a H_2-Br_2 fuel cell and the results are presented in Figures 14 and 15. In this study, a mixture of 2 M HBr and 0.9 M Br_2 was recirculated through the bromine electrode at different flow rates. Figure 14 shows the performance of the fuel cell under the operating conditions described in the Experimental section with 3 layers of the conventional SGL 10AA electrode at 10 cc/min/cm^2, 1 layer of MWCNT-based carbon electrode at 5 and 10 cc/min/cm^2, and 3 layers of MWCNT electrode at 10 cc/min/cm^2. The MWCNT-based carbon electrode used in the study is the sample labeled CVD 45 (sample 2: 15X active surface area after durability measurements). This sample was chosen as it has the highest active surface area of all the samples synthesized using solution A (in the electrodeposition step) after the durability measurements. Prior to collecting the data for the polarization curve, multiple discharge and charge cycles were carried out to hydrate the membrane electrode assembly (MEA).

The results in Figure 14 show that the fuel cell with a single layer of MWCNT-based carbon electrode exceeded the performance of 3 layers of the conventional SGL 10AA electrode (~12% higher current and power density at 80% discharge efficiency) even at half the flow rate during both discharge and charge. This higher performance acquired with fewer Br_2 electrodes will increase the power output, reduce the size and lower the cost of the fuel cell system. These results are consistent with previous results obtained with lower HBr concentrations.[15] As shown in Figure 14, since a single layer of MWCNT-based carbon electrode has sufficiently high surface area to give good performance, adding more layers of MWCNT electrode (3 layers in this case) would only increase the ionic transport distance (ohmic resistance) in the cell and result in poorer performance, as observed previously by Cho et al.[22] when more than 3 layers of conventional electrodes were used in the bromine side of the cell. Also, the multiple electrode layers used in the fuel cell system result in an additional cost.

A new H_2-Br_2 fuel cell using sample 3 (29X active surface area enhancement after durability measurements) as the Br_2 electrode was tested at different HBr/Br_2 flow rates. Of all the samples synthesized using solutions A and B (electrodeposition step), sample 3 was found to possess the highest active surface area and durability. Also, 3 layers of plain SGL 10AA have been tested and their performance is compared to that of the new MWCNT-based carbon electrode with high durability. As shown in Figure 15, the discharge performance obtained with a single layer of MWCNT-based carbon electrode (sample 3) at a low flow rate (2 cc/min/cm^2) matched that obtained with 3 layers of plain SGL 10AA carbon electrode at a high flow rate (10 cc/min/cm^2). Also, better discharge performance was obtained when the H_2-Br_2 fuel cell system with the MWCNT-based carbon electrode was operated at high flow rates (7 and 10 cc/min/cm^2). For example, at 80% discharge efficiency, the current and power density of H_2-Br_2 fuel cell system acquired with the MWCNT-based carbon electrode is approximately 16% higher than that acquired with 3 layers of plain SGL 10AA carbon electrode.

There are two ways to use MWCNT-based carbon electrodes to gain cost advantages. The first option is to operate a H_2-Br_2 fuel cell with the MWCNT-based carbon electrode at low flow rates so that it matches the fuel cell performance obtained with multiple plain carbon electrodes. This option reduces pumping costs and possibly the bromine electrode cost as well. A detailed cost analysis from the materials perspective will be shown in the next section to determine whether there is a cost advantage of using a MWCNT-based carbon electrode instead of the plain ones. The second option is to operate a H_2-Br_2 fuel cell with the MWCNT-based carbon electrode at high flow rates so that it exceeds the fuel cell performance obtained with multiple plain carbon electrodes. While this option doesn't reduce the pumping costs, it reduces the material and fuel cell stack costs, which is very significant. Since higher fuel cell performance could be obtained with MWCNT-based carbon electrodes, the number of fuel cells in a stack can be reduced for a required stack power.

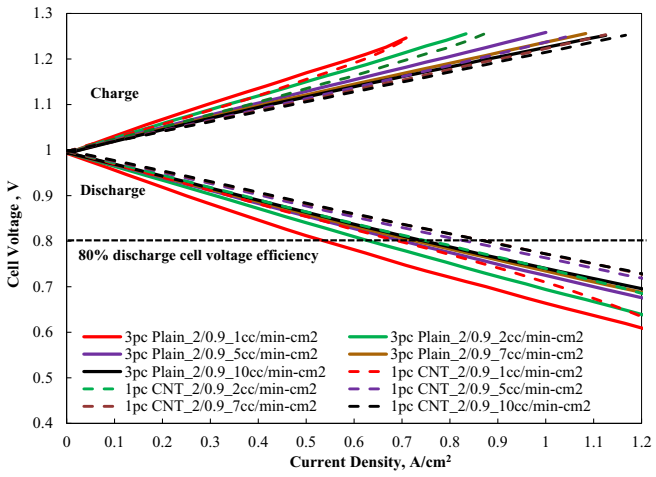

Figure 15. Polarization curves measured during charge and discharge with 3 layers of conventional electrode and 1 layer of MWCNT electrode (sample 3) at different HBr/Br_2 flow rates.

Pressure drop measurements.— Pressure drop measurements were done on both plain SGL 10AA (single layer) and MWCNT-based carbon electrodes (sample 3: Co electrodeposition done using 0.16 M $CoSO_4$) using the procedure described in the Experimental section. Sample 3 was chosen since it is the best performing MWCNT-based carbon electrode. Figure 16 shows the pressure drop across the Br_2 electrode (in cm H_2O) as a function of H_2O flow rate. This is a

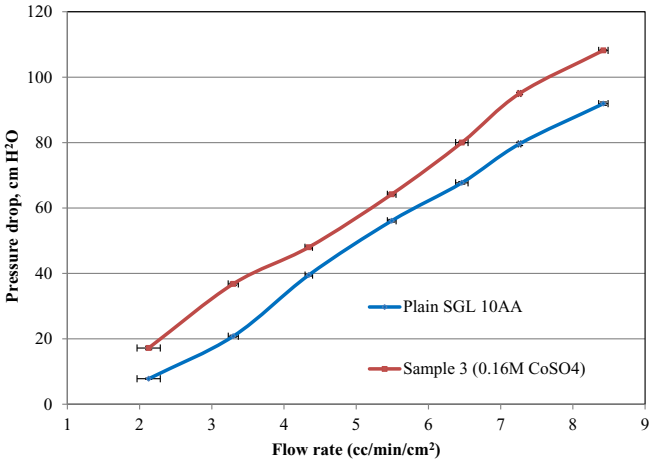

Figure 16. Pressure drop measurements of plain SGL 10AA (single layer) and sample 3 (synthesized at 0.16M $CoSO_4$) MWCNT electrodes at different H_2O flow rates.

comparative study since the pressure drop related to the minor losses in the tubing was included in the total pressure drop measured for both plain SGL 10AA and MWCNT-based carbon electrodes. The pressure drop curves shown in the graph were obtained after multiple measurements. Also, the uncertainties in the flow rates were represented by the error bars.

As shown in Figure 16, the pressure drop with a MWCNT-based electrode is higher than that observed with plain SGL 10 AA (single layer) carbon electrode. The high pressure drop seen in the MWCNT-based carbon electrode might be a result of slight decrease in porosity due to the MWCNT growth on the carbon electrode fiber surface. The increase in pressure drop seen in MWCNT-based carbon electrode is still insignificant to cause any severe resistance to the fluid flow. This can be attributed to the short nanotubes remaining after being subjected to the fluid shear stress and also the very high porosity of SGL 10 AA carbon electrode material compared to the other commercially available ones (Toray, Avcarb, etc.).

Table VI. Electrode properties (AA material) and CNT synthesis costs.

Electrode properties	
Thickness of SGL 10AA carbon electrode	415 μm
Gravimetric BET area of plain carbon electrode (AA material)[a]	0.65 m^2/g
BET area per unit volume of plain carbon electrode (AA material)[b]	0.16 m^2/cm^3
BET density of plain carbon electrode (AA material)	0.25 g/cm^3
Electrodeposition costs	
Cost of plain carbon electrode (10AA)[c]	70 $\$/m^2$
Cost of cobalt sulfate required per gm of carbon electrode	0.00025 $/g of GDL
Cost of boric acid required per gm of carbon electrode[d]	0.000012 $/g of GDL
Cost of electricity per gm carbon electrode[d]	0.0083 $/g of GDL
CVD costs	
Cost of acetylene required per gm of carbon electrode[e]	0.00089 $/g of GDL
Cost of argon required per gm of carbon electrode[e]	0.026 $/g of GDL
Cost of hydrogen required per gm of carbon electrode[e]	0.005 $/g of GDL
Cost of electricity required per gm of carbon electrode[e]	0.225 $/g of GDL

[a]Obtained from Ref. 22.
[b]Obtained from Ref. 19.
[c]Obtained from Ref. 23.
[d]Calculated using information obtained from Ref. 24.
[e]Calculated using information obtained from Ref. 25.

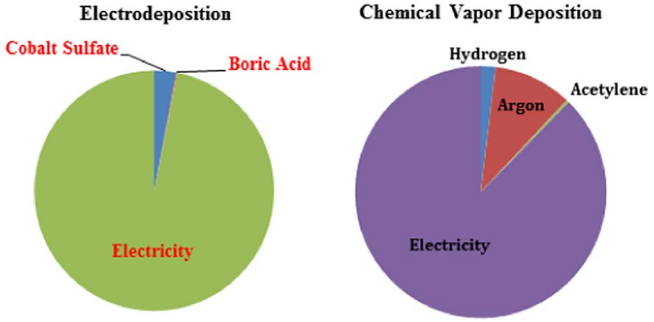

Figure 17. Material costs involved with electrodeposition and chemical vapor deposition processes.

Cost analysis.— A preliminary cost analysis was performed to highlight the cost advantage of using MWCNT electrodes instead of commercially available carbon electrodes. In this study, commercially available SGL 10 AA carbon electrode material was chosen because of their high porosity. The electrode properties of AA material and MWCNT synthesis costs were specified in Table VI. Figure 17 shows pie charts representing the electrodeposition and CVD costs. As shown in Figure 17, electricity was identified to be the major cost factor in both electrodeposition and CVD processes.

There are two cost benefits of using MWCNT-based carbon electrodes. The first benefit of using a MWCNT-based carbon electrode is as follows. In the case with plain porous carbon materials, an electrode with a certain thickness, or multiple layers of thinner electrodes, is needed for each H_2-Br_2 fuel cell in a stack to create the required active surface area to achieve optimal fuel cell performance. Electrode thickness is a limiting factor because mass transport limitation is reached beyond a certain value. However, in the case with porous MWCNT-based carbon materials, one can use a thinner MWCNT-based carbon electrode to obtain the same active area as in the thicker plain electrode. The advantages resulting from this approach are better performance due to shorter mass transport distance and lower ohmic resistance. Another advantage is lower cost if the cost of a single MWCNT-based carbon electrode is lower than the cost of a thicker plain electrode. A case study was conducted to evaluate this point.

In the case of SGL 10AA material frequently used in literature, it was found that using three pieces of plain 10 AA resulted in optimal performance of the H_2/Br_2 fuel cell. As the plain carbon electrodes have low specific surface areas, multiple layers (3 in this case) or thick electrodes are required to enhance the fuel cell performance. The thickness of a single layer of SGL 10 AA is 0.0415 cm. In order to obtain a better understanding of plain carbon electrode thickness to growing multi-walled carbon nanotubes, a plot (Figure 18) has been generated for the cost ratio (ratio of the cost of MWCNT-based carbon electrode which involves both the cost of plain electrode used for MWCNT synthesis as well as the electrodeposition and CVD cost for the respective electrode to the cost of a 0.1245 cm thick plain electrode) versus thickness of MWCNT-based carbon electrode. The cost ratio is calculated using equation 1. The geometric area of the electrode is kept constant as the thickness is varied. Note that there are plain carbon electrodes with high porosity and wide range of thicknesses available in the market (SGL, Toray, Avcarb, etc.).

$$\textit{Cost ratio} = \frac{\textit{Cost of MWCNT based carbon electrode at the respective thickness}}{\textit{Cost of a 0.1245 } (3 \times 0.0415 \textit{ cm}) \textit{ cm thick plain carbon electrode}} \quad [1]$$

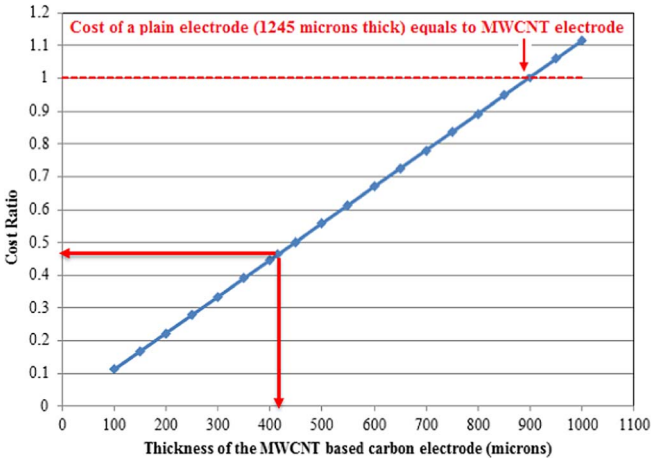

Figure 18. Cost ratio versus thickness of a MWCNT-based carbon electrode.

From Figure 18, we can see that using an electrode with thickness beyond 900 microns offers no cost advantage for the MWCNT-based carbon electrode compared to the cost of a thick plain electrode. The cost ratio exceeding 1 indicates that the cost of the MWCNT-based carbon electrode is higher than that of the plain electrode. On the other hand, the cost is reduced when a thinner MWCNT-based carbon electrode is used. For example, by using a 415 micron thick MWCNT-based carbon electrode, same as one layer of SGL 10AA plain electrode, the cost of a MWCNT-based carbon electrode is about 47% that of a plain carbon electrode of 1245 micron thickness. We could use an even thinner MWCNT-based carbon electrode to obtain a lower cost if the thinner MWCNT-based carbon electrode has equal or higher surface area than the thicker plain electrode. A 20X increase in surface area by this method means we could use a MWCNT-based carbon electrode with a thickness of 62.2 microns. This 62.2 micron thick MWCNT-based carbon electrode should give us the same or better performance at about $1/15^{th}$ the cost of a thicker plain electrode. As reported in the last section, using a single MWCNT-based 10AA carbon electrode resulted in higher performance than three layers of 10AA plain electrode. This shows both performance and cost advantages.

The second benefit is that the performance enhancement resulting in the usage of a MWCNT-based carbon electrode might enable us to reduce the number of H_2/Br_2 fuel cells required per stack of a given power rating. This approach could result in a significant cost reduction when fewer more expensive components like membrane, catalyst, bipolar plates, gas diffusion layers, MEA frames, gaskets, endplates, etc. are used in the fuel cell stack. Also, the size and weight of the fuel cell stack are reduced due to using thinner CNT electrodes in each cell resulting in higher volumetric and gravimetric stack power densities. The enhancement in discharge performance (at 80% discharge efficiency) with a single layer of (0.0415 cm thickness) MWCNT electrode was 16%. So, for every 7 fuel cells employing thicker plain carbon electrodes in a stack, one entire fuel cell could be eliminated by employing thinner MWCNT-based carbon electrodes. For a required stack power, the number of cells in a stack can be reduced by 16% using MWCNT-based carbon electrodes.

Conclusions

In this study, MWCNT-based carbon electrodes with high surface area and durability were synthesized using modified electrodeposition and CVD experimental configurations. It was found that tall MWCNTs were quickly lost once they were exposed to high fluid flow rates. Smaller Co nanoparticles with dense distribution were obtained by lowering the $CoSO_4$ concentration. The durability of carbon electrodes with a dense distribution of short MWCNTs was found to be ideal against high liquid flow rates. The higher fuel cell performance obtained with MWCNT-based carbon electrodes was expected to lower the fuel cell system cost. The increase in pressure drop in the MWCNT-based carbon electrode is insignificant relative to the untreated electrode used as the substrate. The preliminary cost analysis has shown that the CNT electrode material could provide significant cost advantages over conventional porous gas diffusion electrode materials. Finally, these MWCNT-based carbon electrodes can also be used in various flow battery/reversible fuel cell systems (e.g. All Vanadium, Fe-Cr, Zn-Br_2 etc.) that need porous carbon electrodes with high active surface area.

Acknowledgments

The authors acknowledge the financial support of this work by the National Science Foundation through grant no. EFRI-1038234 and ARPA-E program under Department of Energy through grant number AR0000262.

References

1. T. Nguyen and R. Savinell *Electrochemical Society Interface*, **19**(3), 54 (2010).
2. W. Glass and G. H. Boyle, *Advances in Chemistry Series*, **47**, 203 (1965).
3. R. S. Yeo and D. T. Chin, *J. Electrochem. Soc.*, **127**(3), 549 (1980).
4. G. G. Barna, S. N. Frank, T. H. Teherani, and L. D. Weedon, *J. Electrochem. Soc.*, **131**(9), 1973 (1984).
5. V. Livshits, A. Ulus, and E. Peled, *Electrochemistry communications*, **8**, 1358 (2006).
6. K. T. Cho, P. Ridgeway, A. Z. Weber, S. Haussener, V. Battagalia, and V. Srinivasan, *J. Electrochem. Soc.*, **159**(11), A1806 (2012).
7. H. Kreutzer, V. Yarlagadda, and T. V. Nguyen, *J. Electrochem Soc.*, **159**(7), F331 (2012).
8. Michael C. Tucker, K. T. Cho, A. Z. Weber, G. Lin, and T. V. Nguyen, *J. Appl. Electrochem.*, **45**, 11 (2015).
9. A. Ivanovskaya, N. Singh, R.-F. Liu, H. Kreutzer, J. Baltrusaitis, T. V. Nguyen, H. Metiu, and E. McFarland, *Langmuir*, **29**, 480 (2013).
10. T. V. Nguyen, H. Kreutzer, V. Yarlagadda, E. McFarland, and N. Singh, *ECS Transactions*, **53**(7), 75 (2013).
11. V. Yarlagadda, R. P. Dowd Jr., J. W. Park, P. N. Pintauro, and T. V. Nguyen, *J. Electrochem. Soc.*, **162**(8), F919 (2015).
12. J. W. Park, R. Wycisk, and P. N. Pintauro, *ECS Transactions*, **50**(2), 1217 (2012).
13. J. W. Park, R. Wycisk, and P. N. Pintauro, *J. Memb. Sci.*, **490**, 103 (2015).
14. V. Yarlagadda and T. V. Nguyen, *ECS Transactions*, **58**(36), 25 (2014).
15. V. Yarlagadda, G. Lin, P. Y. Chong, and T. Van Nguyen, "High Surface Area Carbon Electrodes for Bromine Reactions in H_2-Br_2 Fuel Cell," *J. Electrochem. Soc.* To be published (2015).
16. C. Wang, M. Waje, X. Wang, J. M. Tang, R. C. Haddon, and Y. Yan, *Nano Letters*, **4**(2), 345 (2004).
17. C. Du, B. Wang, and X. Cheng, *J. Power Sources*, **187**, 505 (2009).
18. B. Kim, H. Chung, and W. Kim, *J. Phys. Chem. C.*, **114**, 15223 (2010).
19. S. C. Barton, Y. Sun, B. Chandra, S. White, and J. Hone, *Electrochemical and Solid-State Letters*, **10**(5), B96 (2007).
20. T. Nguyen, *J. Electrochem. Soc.*, **143**, L103 (1996).
21. M. S. Chandrasekar and M. Pushpavanam, *Electrochimica Acta*, **53**, 3313 (2008).
22. C.-N. Sun, F. M. Delnick, D. S. Aaron, A. B. Papandrew, M. M. Mench, and T. A. Zawodzinski, *ECS Electrochemistry Letters*, **2**(5), A43 (2013).
23. Kyu Taek Cho, Paul Albertus, Vincent Battaglia, Aleksander Kojic, Venkat Srinivasan, and Adam Z. Weber, *Energy Technol.*, **1**, 596 (2013).
24. http://www.icis.com/chemicals/channel-info-chemicals-a-z/
25. http://bgs.vermont.gov/sites/bgs/files/pdfs/purchasing/Airgas-Price-List.pdf